



ELSEVIER




Contents lists available at ScienceDirect

Mechanism and Machine Theory

journal homepage: www.elsevier.com/locate/mechmt

Research paper

Driving rotational motion with Euler parameters: a constraint formulation for multibody systems

 Madalena Antunes ^{*} , João Folgado , Carlos Quental 

IDMEC, Instituto Superior Técnico, Universidade de Lisboa, Av. Rovisco Pais 1, 1049-001, Lisbon, Portugal

ARTICLE INFO

Keywords:

 Multibody system
 Kinematic constraint
 Rotational driver
 Euler parameters
 Redundancy
 Biomechanical model

ABSTRACT

The formulation of rotational driving constraints using angular variables (angle-based formulation) may introduce numerical instabilities and redundancy among kinematic constraints, which can compromise the robustness of multibody analyses. This study proposes an alternative Euler-based formulation, in which Euler parameters, describing the relative orientation between joint-connected bodies, are used to define rotational driving constraints. This formulation avoids singularities, enables full range of motion evaluation, and eliminates redundancy. Both angled-based and Euler-based formulations were applied to different joints within both open and closed kinematic chains using an in-house multibody model of the human body. Kinematic and inverse dynamic analyses were conducted across several movements from multiple subjects, and the results were compared between the two formulations and literature data. The Euler-based formulation provided independent kinematic constraints and showed good agreement with joint kinematics and torques from established methods. In addition, it improved computational efficiency. Overall, the use of Euler parameters offers a robust and efficient alternative to angle-based formulations for rotational driving constraints in multibody system dynamics.

1. Introduction

The analysis of human motion using multibody systems provides valuable insights into the kinematics and dynamics of body segments and joints [1–3]. In biomechanics, most applications focus on inverse dynamic analyses, which rely on the availability of known motion data to estimate interactions between bodies, such as joint torques and joint reaction forces [4]. Optoelectronic marker-based systems using retro-reflective markers are considered the gold standard method for motion acquisition [4]. However, despite their high accuracy, these systems are subjected to several error sources, such as soft tissue artifacts, which impact estimates of body segment lengths, joint motion, and other variables, and can propagate through the model, potentially compromising the accuracy of biomechanical analyses. To address this, the acquired data are usually used as prescribed input for kinematic analyses, which compute positions, velocities, and accelerations that are consistent with the kinematic constraints of the multibody system [5]. These constraints include joint constraints, which define the geometric relationships between the bodies connected by joints (kinematic pairs), as well as driving constraints, which guide the degrees of freedom (DoFs) of the system over time using the prescribed data [3,6,7]. In kinematic analyses, the system must be fully defined, i.e., the number of independent kinematic constraints must be equal to the number of generalized coordinates. Fewer independent constraints produce an underdetermined system, while more constraints

* Corresponding author: IDMEC, Instituto Superior Técnico, Universidade de Lisboa, Av. Rovisco Pais 1, 1049-001, Lisbon, Portugal.

E-mail addresses: madalena.antunes@tecnico.ulisboa.pt (M. Antunes), jfolgado@tecnico.ulisboa.pt (J. Folgado), carlos.quental@tecnico.ulisboa.pt (C. Quental).

<https://doi.org/10.1016/j.mechmachtheory.2025.106315>

Received 17 October 2025; Received in revised form 27 November 2025; Accepted 2 December 2025

Available online 10 December 2025

0094-114X/© 2025 The Author(s).

Published by Elsevier Ltd. This is an open access article under the CC BY license (<http://creativecommons.org/licenses/by/4.0/>).

Nomenclature

Abbreviations

2D	Two-dimensional
3D	Three-dimensional
AC	Acromioclavicular
Angle-based	Rotational driving constraint based on angle parameters
DoF	Degree of Freedom
Euler-based	Rotational driving constraint based on Euler parameters
GH	Glenohumeral
HU	Humeroulnar
ISB	International Society of Biomechanics
JCS	Joint Coordinate System
LBL	Lisbon Biomechanics Laboratory
RC	Radiocarpal
RoM	Range of Motion
RU	Radioulnar
SC	Sternoclavicular
ST	Scapulothoracic

Latin Symbols

\mathbf{A}_k	Rotational transformation matrix of body k (-)
e_0, e_1, e_2 and e_3	Entries of the Euler parameters (-)
$e_{0ij}, e_{1ij}, e_{2ij}$ and e_{3ij}	Entries of the relative Euler parameters (-)
\mathbf{g}	Vector of generalized external forces (N, N.m)
\mathbf{G}_k	3×4 transformation matrix for body k (-)
i	Body i (-)
\mathbf{I}	Identity matrix (-)
j	Body j (-)
\mathbf{L}_k	3×4 transformation matrix for body k (-)
\mathbf{M}	Mass matrix of the multibody system (kg, kg.m ²)
\mathbf{p}_i	Vector of four Euler parameters (-)
\mathbf{p}_{ij}	Vector of four relative Euler parameters (-)
\mathbf{q}	Vector of generalized positions of the system (m)
$\dot{\mathbf{q}}$	Vector of generalized velocities of the system (m.s ⁻¹ , rad.s ⁻¹)
$\ddot{\mathbf{q}}$	Vector of generalized acceleration of the system (m.s ⁻² , rad.s ⁻²)
\mathbf{r}_k	Global components of the position vector for body k (m)
\mathbf{s}_k	Global components of vector \mathbf{s} belonging to body k (m)
\mathbf{s}'_k	Body-fixed components of vector \mathbf{s} belonging to body k (m)
$\tilde{\mathbf{s}}_k$	3×3 skew-symmetric matrix (m)
$\bar{\mathbf{s}}_k$	4×4 skew-symmetric matrix containing a negative 3×3 skew-symmetric matrix (m)
$\hat{\mathbf{s}}_k$	4×4 skew-symmetric matrix containing a positive 3×3 skew-symmetric matrix (m)
\mathbf{v}	Four-dimensional column vector (-)
xyz	Global fixed coordinate system (-)

Greek Symbols

γ	Right-hand side vector of the acceleration equations of the system (-)
θ	Angle between bodies i and j (rad)
λ	Vector of Lagrange multipliers (-)
ν	Right-hand side vector of the velocity equations of the system (-)
$\xi\eta\zeta$	Body-fixed coordinate system (-)
$\Phi, \dot{\Phi}, \ddot{\Phi}$	Kinematic constraints and its first and second derivatives with respect to time (-)
$\Phi_{\mathbf{q}}$	Jacobian matrix of the kinematic constraints (-)
ω	Angular velocities in global coordinates (rad.s ⁻¹)
ω'	Angular velocities in local coordinates (rad.s ⁻¹)
$\dot{\omega}$	Angular accelerations in global coordinates (rad.s ⁻²)
$\dot{\omega}'$	Angular accelerations in local coordinates (rad.s ⁻²)

introduce redundancy.

Overall, joint constraint equations are well established in the literature [3,8–10]. However, the formulation of driving constraints is less standardized. When reported, the main types involve prescribing the position of a body, the distance between bodies, or the relative rotation between bodies over time [3,7]. Among these, prescribing the relative rotation between bodies is one of the most common types of drivers used. This is often implemented by defining the angle between two-unit vectors, each fixed to one of the bodies, and prescribing its time-dependent variation through a constraint equation based on the dot-product of the vectors [11–14]. However, this formulation presents an important limitation: when the angle between the vectors approaches 0° or 180° , they become aligned (in the same or opposite direction), leading to numerical instabilities [15]. One way to address this issue is to restrict the range of motion (RoM) by removing time intervals where the guided joint angles approach these critical angles. This solution disrupts the continuity of motion and excludes frames that may be relevant for biomechanical interpretation. Therefore, it is often an unpractical option. Alternatively, a second rotational driving constraint can be introduced to guide the same DoF, using a different pair of vectors that remain well separated when the primary constraint nears these critical angles. While this solution allows the full RoM to be evaluated, it introduces redundancy in the kinematic constraints, which must be managed to ensure accurate analyses [3,16].

To address redundancy, specialized strategies are required depending on the type of analysis. In kinematic analyses, an iterative Newton-Raphson method coupled with a least square approach may be used to find consistent solutions [17,18]. In inverse dynamics, the equations of motion may be solved as an optimization problem, as often performed with detailed musculoskeletal models for which the number of unknown muscle forces exceeds the number of DoFs of the system, allowing the solution to accommodate dependent constraints without instability. In forward dynamics, redundancy directly affects the integration of the equations of motion. To address this, specialized methodologies, such as generalized coordinate partitioning [19], augmented Lagrangian formulations [20–22], or penalty-based formulations [23,24], are employed, generally relying on more elaborate formulations to ensure numerical stability and accurate integration over time.

Given the limitations associated with the use of angular variables in rotational driving constraints, alternative formulations are of significant relevance. An alternative to angle-based formulations is the use of Euler parameters. The concept of Euler parameters dates to Euler's rotation theorem in 1775, which established that any rotation in the three-dimensional space can be represented as a single rotation about a fixed axis [25]. Subsequent developments by Rodrigues, Hamilton, and Gauss expanded on Euler's work, further defining their mathematical properties and relationships [26,27]. From the 1960s onwards, Euler parameters were increasingly adopted in multibody dynamics because of their computational advantages [3,15,28,29]. Compared to angular representations, Euler parameters offer several benefits: they avoid singularities, lead to more compact kinematic constraint equations, and enable more computationally efficient formulations [8,30]. Building on these advantages, Nikravesh proposed in 1988 using Euler parameters to describe the relative orientation of a kinematic pair about a relative axis of rotation [3]. When used in this way to describe the orientation of a body relative to another body about a relative axis of rotation, this formulation has been referred to as relative Euler parameters [14,31–33], a term adopted throughout this paper. To date, this formulation seems to have been applied as a rotational driving constraint in only one study; however, it did not provide a detailed description of the driving constraint equation used, it was limited to revolute and spherical joints in open kinematic chains, and it did not avoid redundancy in the kinematic constraints [14].

This study proposes an alternative to angle-based rotational driving constraints that addresses their singularity and redundancy issues by using relative Euler parameters to define rotational drivers in a more robust and numerically stable way. To evaluate this formulation, hereafter referred to as Euler-based, kinematic and dynamic analyses were conducted using both the angle- and Euler-based formulations, and their results were compared to literature data when available. These analyses used an in-house multibody model of the human body, incorporating various joint types within both open and closed kinematic chains [34,35]. Although the proposed formulation was tested in the context of biomechanics, it is generally applicable to multibody modelling.

This paper is organized as follows: Section 2 presents a brief review of kinematics and inverse dynamics in multibody system dynamics; Section 3 presents the rotational driving constraint equations — both angle- and Euler-based formulations — along with their respective derivatives required for kinematic and dynamic analyses; Section 4 describes the multibody model used along with the implementation of the angle- and Euler-based formulations, and outlines the methodology followed to compute joint angles and torques; Section 5 presents and discusses the results obtained from the kinematic and dynamic analyses performed; and, finally, Section 6 summarizes the main advantages of the proposed formulation and concludes the work. Additional definitions and derivations related to Euler and relative Euler parameters are provided in Appendices A and B.

2. Multibody system dynamics methodology

This work uses Cartesian coordinates to specify the location of a body-fixed reference frame (x , y and z) and four rotational coordinates (Euler parameters) to define its orientation (ξ , η and ζ) with respect to the global reference frame [3,25,29]. For each frame, or time instant, the configuration (position and orientation) of all bodies within a multibody system are grouped in the vector of generalized coordinates \mathbf{q} [9,36].

The generalized coordinates are often dependent, with their relationships described by algebraic equations, commonly referred to as kinematic constraint equations and denoted by Φ [9,37]. These equations typically reflect the geometric relationships imposed by joints as well as any driving conditions used to control the system's DoFs [3,7–10]. In a kinematic analysis, all DoFs must be properly guided [3,16]. The consistent positions, which satisfy the kinematic constraints of the multibody system, are determined by solving the following system of non-linear equations over time:

$$\Phi(\mathbf{q},t) = \mathbf{0} \quad (1)$$

Having the consistent positions determined, the consistent velocities and accelerations, for each time instant, can be obtained through the differentiation of the kinematic constraint equations with respect to time [6]. The first differentiation of Eq. (1) yields:

$$\begin{aligned} \dot{\Phi}(\mathbf{q}, t) &= \Phi_{\mathbf{q}}\dot{\mathbf{q}} + \frac{\partial\Phi}{\partial t} = \mathbf{0} \Leftrightarrow \Phi_{\mathbf{q}}\dot{\mathbf{q}} = \boldsymbol{\nu} \\ \boldsymbol{\nu} &= -\frac{\partial\Phi}{\partial t} \end{aligned} \tag{2}$$

where $\Phi_{\mathbf{q}}$ is the Jacobian matrix of the kinematic constraint equations, $\dot{\mathbf{q}}$ are the generalized velocities of the system, and $\boldsymbol{\nu}$ is the right-hand side vector of the velocity constraint equations. The second differentiation of Eq. (1), or first differentiation of the velocity constraint equations, yields:

$$\begin{aligned} \ddot{\Phi}(\mathbf{q}, t) &= \Phi_{\mathbf{q}}\ddot{\mathbf{q}} + (\Phi_{\mathbf{q}\dot{\mathbf{q}}})_{\mathbf{q}}\dot{\mathbf{q}} + 2\Phi_{\mathbf{q}t}\dot{\mathbf{q}} + \frac{\partial^2\Phi}{\partial t^2} = \mathbf{0} \Leftrightarrow \Phi_{\mathbf{q}}\ddot{\mathbf{q}} = \boldsymbol{\gamma} \\ \boldsymbol{\gamma} &= -(\Phi_{\mathbf{q}\dot{\mathbf{q}}})_{\mathbf{q}}\dot{\mathbf{q}} - 2\Phi_{\mathbf{q}t}\dot{\mathbf{q}} - \frac{\partial^2\Phi}{\partial t^2} \end{aligned} \tag{3}$$

where $\ddot{\mathbf{q}}$ is the vector of generalized accelerations of the system, $\boldsymbol{\gamma}$ is the right-hand side vector of the acceleration constraint equations, and $\Phi_{\mathbf{q}t}$ represents the partial derivatives of the kinematic constraint equations with respect to the generalized coordinates and time.

Although Euler parameters are well suited for representing a body's angular orientation, their use leads to an excessive number of equations when time derivatives are considered [30]. To mitigate this, the velocity and acceleration equations may be expressed in terms of angular velocities $\boldsymbol{\omega}'$ and accelerations $\boldsymbol{\omega}'$, while still preserving the advantages of Euler parameters [8,30]. Here, the superscript (') indicates that angular velocities and accelerations are expressed in the body-fixed reference frames.

The dynamics of a constrained multibody system is governed by equations of motion that relate the generalized forces and moments to the kinematics of the system [5,6,9,28,37,38]. These equations can be written as:

$$\mathbf{M}\ddot{\mathbf{q}} + \Phi_{\mathbf{q}}^T\boldsymbol{\lambda} = \mathbf{g} \tag{4}$$

where \mathbf{M} is the mass matrix of the system, including mass and moment of inertia for each body; \mathbf{g} is the vector of generalized external forces; and $\boldsymbol{\lambda}$ is the vector of Lagrange multipliers, associated with the kinematic constraints of the system. The terms $\mathbf{M}\ddot{\mathbf{q}}$ and $-\Phi_{\mathbf{q}}^T\boldsymbol{\lambda}$ represent the inertial and internal forces of the system, respectively [3,5,16]. When drivers from the kinematic analysis are included in the constraint equations, their reaction forces generate motion. As in inverse dynamics, positions, velocities, and accelerations are known, the Lagrange multipliers are the only unknowns to be determined from the equations of motion [3,16]. For a multibody system with no redundant constraints, the Lagrange multipliers can be obtained by

$$\boldsymbol{\lambda} = [\Phi_{\mathbf{q}}^T]^{-1}(\mathbf{g} - \mathbf{M}\ddot{\mathbf{q}}) \tag{5}$$

However, in the presence of redundant kinematic constraints, the number of unknowns exceeds the number of generalized coordinates, so the system becomes underdetermined. In this case, the equations of motion can be solved as an optimization problem that yields a consistent set of Lagrange multipliers [3,16].

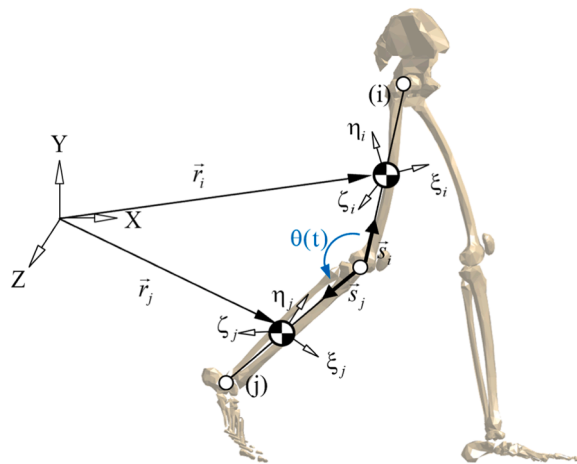


Fig. 1. Schematic representation of an angle-based rotational driver between bodies i and j . The angle $\theta(t)$ represents the prescribed angle between the two vectors.

3. Rotational driving constraints

Having established the general framework for kinematic and dynamic analyses, the focus now shifts to the formulation of rotational driving constraints, which prescribe the relative rotation between two bodies connected by a kinematic joint. These constraints are included in the kinematic constraints (Φ) and can be formulated using angles or, as proposed in this work, using relative Euler parameters. In this section, both formulations are presented, and the corresponding equations required for the multibody system dynamic methodology are derived.

3.1. Angle-based formulation

The angle-based formulation of the rotational driving constraint is defined using two vectors, each fixed to the body-fixed frame of the rigid bodies composing the joint. The relative angle between these vectors is controlled over time by a prescribed angle to enforce the desired movement (Fig. 1).

The angle-based rotational driving constraint equation is referred to as $\Phi^{(A-rot,1)}$, following the notation used by Nikravesh [3], and formulated as

$$\Phi^{(A-rot,1)} = \mathbf{s}_i^T \mathbf{s}_j - \cos\theta(t) = \mathbf{0} \quad (6)$$

$$\mathbf{s}_k = \mathbf{A}_k \mathbf{s}'_k \quad (7)$$

where \mathbf{s}'_k , with $(k = i, j)$, is a unit vector defined in the body-fixed frame of body k . The transformation matrix \mathbf{A}_k relates the body-fixed frame of body k with the global reference frame. Therefore, \mathbf{s}_k represents the orientation of the unit vector in the global reference frame. The time-dependent function $\theta(t)$ represents the prescribed angle used to guide the relative orientation between the vectors.

The contribution of the angle-based rotational driving constraint to the Jacobian matrix is obtained from the partial derivative of Eq. (6) with respect to the generalized coordinates, yielding:

$$\Phi_q^{(A-rot,1)} = [\dots \quad \mathbf{0} \quad 2\mathbf{s}_j^T \mathbf{G}_i \bar{\mathbf{s}}'_i \quad \dots \quad \mathbf{0} \quad 2\mathbf{s}_i^T \mathbf{G}_j \bar{\mathbf{s}}'_j \quad \dots] \quad (8)$$

Matrix \mathbf{G} is a transformation matrix introduced by Nikravesh [3], as presented in detail in Appendix A, and $\bar{\mathbf{s}}$ is a 4×4 skew-symmetric matrix, defined as follows:

$$\bar{\mathbf{s}}_k = \begin{bmatrix} 0 & -\mathbf{s}'_k{}^T \\ \mathbf{s}_k & \tilde{\mathbf{s}}_k \end{bmatrix} \quad (9)$$

In Eq. (9), $\tilde{\mathbf{s}}$ contains a negative 3×3 skew-symmetric matrix $\tilde{\mathbf{s}}_k$, defined as:

$$\tilde{\mathbf{s}}_k = \begin{bmatrix} 0 & -s_{k3} & s_{k2} \\ s_{k3} & 0 & -s_{k1} \\ -s_{k2} & s_{k1} & 0 \end{bmatrix} \quad (10)$$

Expressing the velocity and acceleration equations in terms of angular velocities ω' and accelerations $\dot{\omega}'$, respectively, Eq. (8) can be modified accordingly by using the relationships between the derivatives of the Euler parameters and the angular velocities and accelerations, resulting in:

$$\Phi_q^{(A-rot,1)} = [\dots \quad \mathbf{0} \quad \mathbf{s}_j^T \mathbf{G}_i \mathbf{L}_i \bar{\mathbf{s}}'_i \quad \dots \quad \mathbf{0} \quad \mathbf{s}_i^T \mathbf{G}_j \mathbf{L}_j \bar{\mathbf{s}}'_j \quad \dots] \quad (11)$$

where matrix \mathbf{L} is a transformation matrix, presented in detail in Appendix A [3].

The right-hand side vector of the velocity constraint equations is given by

$$\nu = -\dot{\theta}(t) \sin\theta(t) \quad (12)$$

The contribution of the angle-based rotational driving constraint to the right-hand side vector of the acceleration constraint equations is obtained from the second derivative of Eq. (6) with respect to time, yielding:

$$\gamma = -2\dot{\mathbf{s}}_i^T \dot{\mathbf{s}}_j - \mathbf{s}_i^T (\dot{\mathbf{G}}_j \bar{\mathbf{s}}_j \mathbf{L}_j^T \omega_j'^T) - \mathbf{s}_j^T (\dot{\mathbf{G}}_i \bar{\mathbf{s}}_i \mathbf{L}_i^T \omega_i'^T) - \dot{\theta}(t)^2 \cos\theta(t) - \ddot{\theta}(t) \sin\theta(t) \quad (13)$$

If the acceleration constraint equations are written in terms of angular accelerations, Eq. (13) is modified accordingly:

$$\gamma = -2\dot{\mathbf{s}}_i^T \dot{\mathbf{s}}_j - \mathbf{s}_i^T (\dot{\mathbf{G}}_j \bar{\mathbf{s}}_j \mathbf{L}_j^T \omega_j'^T) - \mathbf{s}_j^T (\dot{\mathbf{G}}_i \bar{\mathbf{s}}_i \mathbf{L}_i^T \omega_i'^T) - \dot{\theta}(t)^2 \cos\theta(t) - \ddot{\theta}(t) \sin\theta(t) + \dots \quad (14)$$

$$\frac{1}{2} \mathbf{s}_j^T \mathbf{G}_i \bar{\mathbf{s}}_i (\omega_i'^T \omega_i') \mathbf{p}_i + \frac{1}{2} \mathbf{s}_i^T \mathbf{G}_j \bar{\mathbf{s}}_j (\omega_j'^T \omega_j') \mathbf{p}_j$$

The first derivative of the unit vector \mathbf{s}_k with respect to the global reference frame can be written as

$$\dot{\mathbf{s}}_k = 2\mathbf{G}_k \bar{\mathbf{s}}_k' \dot{\mathbf{p}}_k = \mathbf{G}_k \bar{\mathbf{s}}_k' \mathbf{L}_k^T \omega_k'^T \quad (15)$$

in which $\dot{\mathbf{p}}_k$ represents the first derivative of the Euler parameters of body k , and ω_k' represents the local components of the angular velocity of body k . These variables are obtained by solving the velocity constraint equations.

3.2. Euler-based formulation

3.2.1. Relative Euler parameters

The Euler parameters provide a non-singular description of the orientation of a body with respect to the global reference frame, around a general axis of rotation. Based on this concept, the relative Euler parameters were introduced to describe the orientation of a body i with respect to a body j [3]. The rotation is described around a relative axis of rotation. The relative Euler parameters are expressed as

$$e_{0ij} = \cos\left(\frac{\varphi}{2}\right) \quad (16)$$

$$\mathbf{e}_{ij} = \mathbf{u} \cdot \sin\left(\frac{\varphi}{2}\right) \quad (17)$$

in which φ is the angle of rotation and \mathbf{u} is a unit vector defining the relative axis of rotation.

The relative Euler parameters can also be written as a function of the Euler parameters of the connected bodies as

$$\mathbf{p}_{ij} = \begin{bmatrix} e_0 \\ \mathbf{e} \end{bmatrix}_{ij} = \begin{bmatrix} \mathbf{P}^T \\ \mathbf{L} \end{bmatrix}_j \mathbf{p}_i = \mathbf{L}_j^* \mathbf{p}_i \quad (18)$$

Additional details of this formulation can be found in Nikravesh [3].

3.2.2. Euler-based driving constraint formulation

The Euler-based formulation of the rotational driving constraint is referred to hereafter as $\Phi^{(E-rot,1)}$ and is mathematically described as follows:

$$\Phi^{(E-rot,1)} = \mathbf{p}_{ij}^T \mathbf{v} - \mathbf{e}^*(t) = \mathbf{0} \quad (19)$$

$$\mathbf{e}^*(t) = \mathbf{p}_{ij}^{*T} \mathbf{v} \quad (20)$$

where \mathbf{p}_{ij} represents the relative Euler parameters, \mathbf{v} is a 4-dimensional column vector, and $\mathbf{e}^*(t)$ is the corresponding prescribed function of time.

Taking the time derivative of Eq. (19) and applying Eq. (18), the contribution of the Euler-based rotational driving constraint to the Jacobian matrix can be written in terms of Euler parameters as:

$$\Phi_q^{(E-rot,1)} = \begin{bmatrix} \dots & \mathbf{0} & \mathbf{v}^T \begin{bmatrix} \mathbf{P}^T \\ \mathbf{L} \end{bmatrix}_j & \dots & \mathbf{0} & \mathbf{v}^T \begin{bmatrix} \mathbf{P}^T \\ -\mathbf{L} \end{bmatrix}_i & \dots \end{bmatrix} \quad (21)$$

For the interested reader, a detailed derivation of Eq. (21) is provided in Appendix B. As in the angle-based formulation, when the velocity and acceleration equations are expressed in terms of angular components, Eq. (19) is modified to:

$$\Phi_q^{(E-rot,1)} = \begin{bmatrix} \dots & \mathbf{0} & \frac{1}{2} \mathbf{v}^T \begin{bmatrix} \mathbf{P}^T \\ \mathbf{L} \end{bmatrix}_j \mathbf{L}_i^T & \dots & \mathbf{0} & \frac{1}{2} \mathbf{v}^T \begin{bmatrix} \mathbf{P}^T \\ -\mathbf{L} \end{bmatrix}_i \mathbf{L}_j^T & \dots \end{bmatrix} \quad (22)$$

The right-hand side vector of the velocity constraint equations is given by:

$$\boldsymbol{\nu} = \mathbf{v}^T \dot{\mathbf{p}}_{ij}^*(t) \quad (23)$$

The contribution of the Euler-based rotational driving constraint to the right-hand side vector of the acceleration constraint equations is obtained from the second derivative of Eq. (19) with respect to time, expressed as:

$$\boldsymbol{\gamma} = \mathbf{v}^T \ddot{\mathbf{p}}_{ij}^*(t) - \mathbf{v}^T \begin{bmatrix} 2\dot{\mathbf{p}}_i^T \dot{\mathbf{p}}_j \\ \dot{\mathbf{L}}_j \dot{\mathbf{p}}_i - \dot{\mathbf{L}}_i \dot{\mathbf{p}}_j \end{bmatrix} \quad (24)$$

If the acceleration constraint equations are written in terms of angular accelerations, Eq. (21) is modified accordingly, resulting in:

$$\boldsymbol{\gamma} = \mathbf{v}^T \ddot{\mathbf{p}}_{ij}^*(t) - \mathbf{v}^T \begin{bmatrix} 2\dot{\mathbf{p}}_i^T \dot{\mathbf{p}}_j \\ \dot{\mathbf{L}}_j \dot{\mathbf{p}}_i - \dot{\mathbf{L}}_i \dot{\mathbf{p}}_j \end{bmatrix} + \frac{1}{4} \mathbf{v}^T \begin{bmatrix} \mathbf{P}^T \\ \mathbf{L} \end{bmatrix}_j (\omega_i'^T \omega_i') \mathbf{p}_i + \frac{1}{4} \mathbf{v}^T \begin{bmatrix} \mathbf{P}^T \\ -\mathbf{L} \end{bmatrix}_i (\omega_j'^T \omega_j') \mathbf{p}_j \quad (25)$$

4. Application example: kinematic and dynamic analyses of the human body

To demonstrate the practical application of the Euler-based driving constraint formulation, kinematic and dynamic analyses were conducted using a multibody model of the human body. The following sections describe the model used, the experimental motion data employed to guide the system, and the procedures for performing kinematic and dynamic analyses.

4.1. Multibody model

The three-dimensional (3D) multibody model used in this study was developed in-house and comprised 26 rigid bodies [34,35]: thorax, pelvis, and right and left clavicle, scapula, humerus, ulna, radius, hand, femur, patella, tibia, talus, foot, and toes (Fig. 2). The relative motion between body segments was constrained by 27 kinematic joints connecting them, modelled as ideal mechanical joints. The sternoclavicular (SC), acromioclavicular (AC), glenohumeral (GH), lumbar, and hip joints were modelled as spherical joints. The scapulothoracic (ST) joints were modelled each by two holonomic constraints that limit the movement of two scapula points over an ellipsoid that represents the rib cage [39]. The humeroulnar (HU), radioulnar (RU), femur-patella, knee, ankle, subtalar, and metatarsophalangeal joints were modelled as revolute joints. Motion at the femur-patella joints was fully described as a function of the knee configuration [40]. The radiocarpal (RC) joints were modelled as universal joints.

The relative DoFs of the multibody model were guided by either angled-based or Euler-based rotational driving constraint equations. In the angle-based formulation, two constraints were defined for each DoF to ensure that the full range of joint motion was covered. The first constraint prescribed the angle between two unit-vectors, s_i and s_{j1} , each fixed to one of the bodies. The second constraint prescribed the angle between vector s_i and another vector s_{j2} , which was defined to be perpendicular to the unit-vector s_{j1} . With this setup, when the angle between s_i and s_{j1} approached 0° , the angle between s_i and s_{j2} approached 90° , thereby avoiding numerical instabilities. Accordingly, spherical, universal, and revolute joints were guided by six, four, and two driving constraints, respectively. For the universal and revolute joints, the vectors used in the constraints were chosen to be perpendicular to the rotation axes. For the spherical joints, the vectors were based on the body-fixed frames of each body.

In the Euler-based formulation, the vector \mathbf{v} determines the behaviour of the driving constraint. While \mathbf{v} can be any generic 4-dimensional column vector, in this work it was used to prescribe individual relative Euler parameters by setting all components

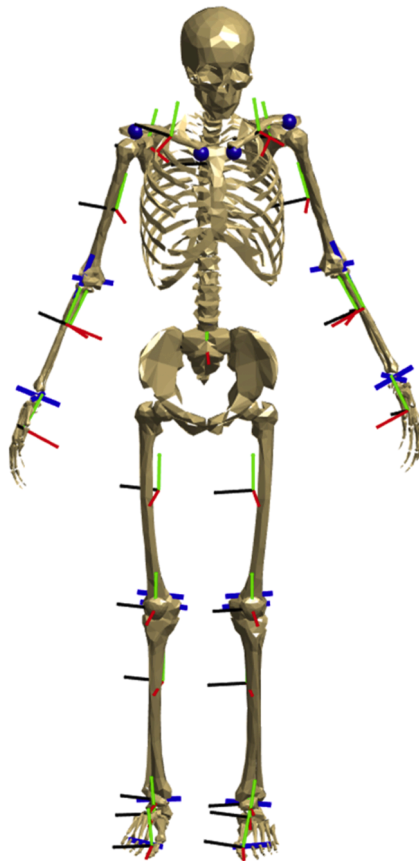


Fig. 2. Geometrical representation of the 3D multibody model used in this study, showing the body-fixed reference frame of each rigid body (ξ -axis in red, η -axis in green, and ζ -axis in black), the centres of spherical joints (blue spheres), and the rotation axes for all other joints (blue lines).

Table 1

Summary of the kinematic joints and the relative Euler parameter components selected to prescribe their motion. Following Nkravesh notation [3], e_{0ij} , e_{1ij} , e_{2ij} , and e_{3ij} correspond to the first, second, third, and fourth components, respectively, of the relative Euler parameters.

Limb	Kinematic Joint	Type of Joint	Relative Euler parameter(s) selected
Upper	Sternoclavicular (SC)	Spherical	e_{1ij} , e_{2ij} and e_{3ij}
	Acromioclavicular (AC)	Spherical	e_{2ij}
	Glenohumeral (GH)	Spherical	e_{1ij} , e_{2ij} and e_{3ij}
	Humeroulnar (HU)	Revolute	e_{3ij}
	Radioulnar (RU)	Revolute	e_{2ij}
	Radiocarpal (RC)	Universal	e_{1ij} and e_{3ij}
Lower	Lumbar	Spherical	e_{1ij} , e_{2ij} and e_{3ij}
	Hip	Spherical	e_{1ij} , e_{2ij} and e_{3ij}
	Knee	Revolute	e_{3ij}
	Ankle	Revolute	e_{3ij}
	Subtalar	Revolute	e_{1ij}
	Metatarsophalangeal	Revolute	e_{3ij}

except one to zero. Spherical, universal, and revolute joints were guided by three, two, and one driving constraint(s), respectively, each associated with a different relative Euler parameter. The selection of which Euler parameter to prescribe was adapted to each joint type based on its mechanics and expected motion. In all cases, the common rationale was to choose the e_{ij} component that dominated in magnitude throughout the joint's RoM, since this component best reflected the joint's primary behaviour.

According to the International Society of Biomechanics (ISB) recommendations, the relative axes of rotation of the HU, knee, ankle, and metatarsophalangeal joints, each modelled as a revolute joint, are generally aligned with the ζ -axis of their respective joint coordinate system (JCS). Accordingly, the parameter e_{3ij} was prescribed, and the vector \mathbf{v} used in the driving constraint (Eq. (19)) was of the form $\mathbf{v} = [0 \ 0 \ 0 \ 1]^T$. For the RU joint, rotations around the η -axis of the forearm define pronation-supination of the radius relative to the ulna; therefore, the component e_{2ij} was selected. The subtalar joint allows inversion-eversion around the ξ -axis of its JCS, so the component e_{1ij} was selected.

For the RC joints, modelled as universal joints, the components e_{1ij} and e_{3ij} of the relative Euler parameters, which are generally aligned with the relative joint rotation axes, were selected. For spherical joints not involved in closed-loop chains (GH, lumbar, and hip joints), all e_{ij} components were prescribed. In contrast, for the SC and AC joints, which are part of a four-DoF closed-loop chain, specific adjustments were made. The SC joint was guided by all e_{ij} components, as the other spherical joints, while the AC joint was guided by a single component, selected based on the dominant component of motion, as only one DoF remained in the closed-loop chain. Across a series of evaluated movements, e_{2ij} consistently represented the dominant component of motion and was therefore used to define the Euler-based rotational driving constraint equation for the AC joint.

Table 1 summarizes the relative Euler parameters selected to be prescribed for each joint of the multibody model used. To assess the influence of parameter selection on joint behaviour, different combinations of prescribed relative Euler parameters were tested for each joint. These analyses aimed to provide guidance for robust application of the Euler-based formulation.

4.2. Experimental motion data

Five movements were acquired from the database of the Lisbon Biomechanics Laboratory (LBL). Four movements involved the upper limbs, and one involved the lower limbs. The upper limb movements included abduction in the frontal plane, forward flexion in the sagittal plane, reaching behind the back, and combing the hair. These were performed by eight participants (4 females, 4 males; mean weight, 70.29 ± 14 kg; mean height, 1.72 ± 0.12 m) and were selected to ensure a wide range of upper limb motion. The lower limb movement consisted of a full right gait cycle from a male subject (75 kg; 1.75 m). Because gait is extensively described in the literature and lower limb joint angles exhibit low inter-subject variability, only one subject was evaluated.

All movements were acquired using an optoelectronic marker-based system (Infrared ProReflex 1000 cameras, Qualisys©, Göteborg, Sweden) with a sampling frequency of 100 Hz and retro-reflective markers placed on anatomical landmarks, following the recommendations of the ISB [41,42]. Marker trajectories were visually inspected using the Qualisys Track Manager 2.9 (Qualisys©) software, and missing data segments were reconstructed through spline interpolation. Further processing was performed in MATLAB (Mathworks Inc., Natick, USA) using an in-house script. Each marker coordinate was filtered using a fourth-order, zero-phase-lag Butterworth low-pass filter. The cut-off frequencies were defined individually for each coordinate through residual analysis [43].

The body-fixed reference frames of each body segment were defined according to ISB recommendations. The non-palpable GH and hip joint centres were estimated using the functional method proposed by Gamage and Lasenby [44] and the predictive method proposed by Hara et al. [45], respectively, both applied to a static trial with the subject standing in the anatomical reference position. In the upper limb movements, scapular motion was tracked dynamically using the acromion marker cluster method [46,47], while the axial rotation of the clavicle was estimated by minimizing the AC joint rotations [48]. The lower limb motion was recorded synchronously with ground reaction forces and centres of pressure, measured using three force plates (AMTI OR 6–7–1000, 508 mm x 464 mm). Ground reaction forces were filtered using a fourth-order, zero-phase Butterworth low-pass filter with a 20 Hz cut-off frequency, while centres of pressure were filtered with a 10 Hz cut-off frequency. For simplicity, the ground reaction forces were applied to the feet only, omitting their application to the toes.

The musculoskeletal model was used in its generic form without subject-specific scaling; the prescribed kinematic data were adapted to the model's geometry, and the kinetic data were scaled according to each subject's body weight relative to that of the model's reference subject. Because of the closed-chain nature of the shoulder girdle, the collected experimental data could not be directly imposed on the model without inconsistencies. To address this, an optimization procedure was applied to determine the clavicle and scapula kinematics that best approximated the measured data while fulfilling the constraints of the multibody model [49]. The data resulting from all these procedures, from acquisition to the optimization of the shoulder kinematics, are hereafter referred to as prescribed data and were used in the rotational driving constraint equations.

4.3. Kinematic and dynamic analyses

To compute positions, velocities, and accelerations consistent with the multibody model, kinematic analyses were performed using both angle- and Euler-based formulations. The position constraint equations, expressed in Eq. (1), were solved using an iterative Newton-Raphson method. The iterations proceeded until the maximum residual error between successive iterations was below 10^{-10} . Although this tolerance is stricter than typically required, it was chosen arbitrarily to enforce tighter convergence and ensure a more rigorous satisfaction of the kinematic constraints. For the angle-based formulation, the Newton-Raphson method was coupled with a least-squares approach to handle redundancy. Small residual errors, or constraint violations, can arise because redundant constraints cannot all be satisfied exactly during the iterative solution. To prioritize the enforcement of joint constraints over driving constraints, weights of 1000 and 1 were arbitrarily assigned, respectively, ensuring that violations of joint constraints were penalized more heavily

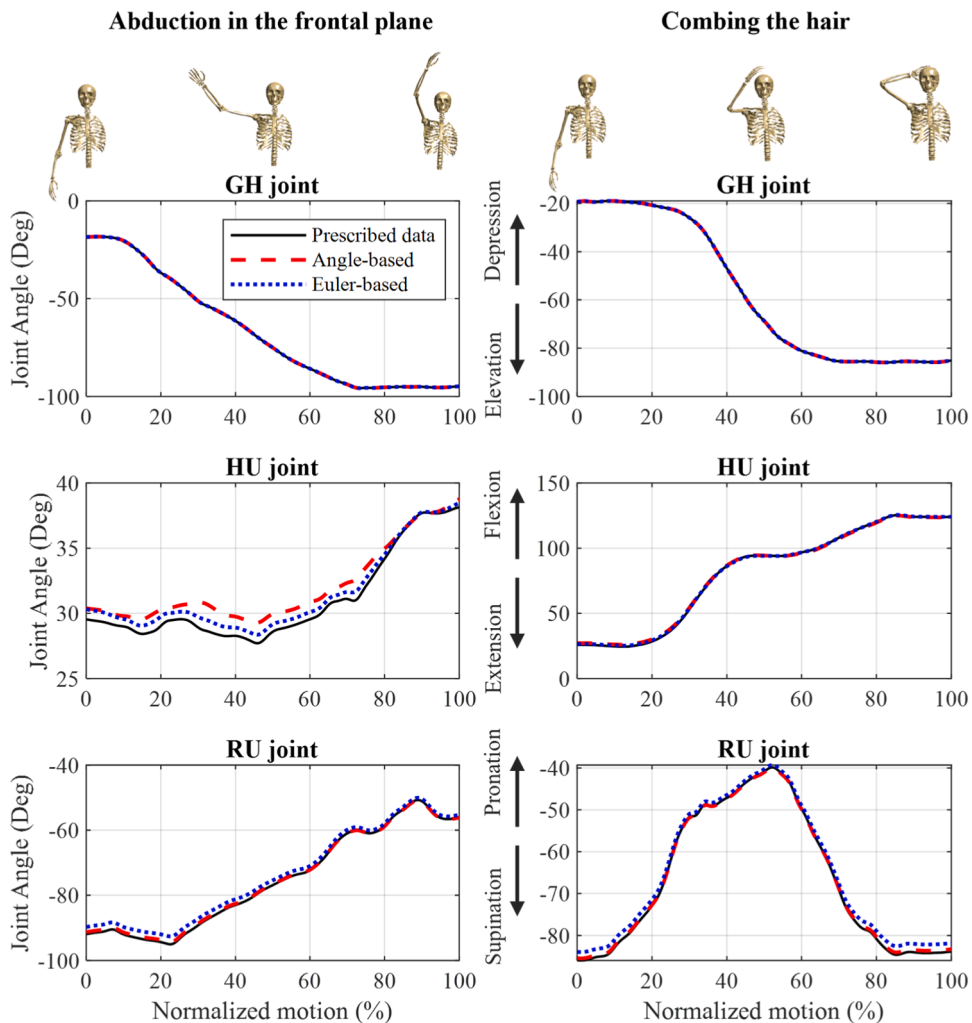


Fig. 3. Elevation-Depression of the Glenohumeral (GH) joint, Flexion-Extension of the Humeroulnar (HU) joint, and Pronation-Supination of the Radioulnar (RU) joint during the movement of abduction in the frontal plane and combing the hair, for the prescribed data and the two conditions tested: angle-based formulation and Euler-based formulation.

than those of driving constraints. From the resulting consistent positions, joint angles were calculated following ISB recommendations [41,42]. The ability of the Euler-based formulation to produce successful anatomical joint motion was evaluated by comparing the main joint angles with those obtained from the prescribed data. For comparison, joint motion derived from the angle-based formulation was also computed. Regarding the lower limbs, the right hip, knee, and ankle joint angles from both formulations were compared with reference data from Winter [50].

Inverse dynamic analyses were performed to evaluate joint torques [34,35], as usually performed in biomechanical analyses [4]. Given the biomechanical model used, which did not include muscles, joint torques were generated from the driving constraints to guide the prescribed motion and ensure dynamic consistency. For both rotational driving constraint formulations, the unknown Lagrange multipliers were computed by solving the equations of motion with MATLAB's *mdivide* function (“\” operator). Accordingly, in the angle-based formulation, a least squares approach was used to handle redundancy. For the upper limb, joint torques were compared between the angle-based and Euler-based formulations. Due to the lack of literature, no additional comparisons were conducted. For the lower limb, in addition to comparing both formulations, joint torques were compared with data from the literature [50]. To assess computational efficiency, simulation (CPU) times for both kinematic and dynamic analyses using the angle-based and Euler-based formulations were recorded. For each movement and analysis, ten simulations were conducted. To mitigate the influence of outliers, the truncated mean was computed by removing the highest and lowest computational times before averaging the remaining values. All simulations were randomized and executed on the same computer (CPU: Intel® Core™ i7–14,700 K, 3.40 GHz up to 5.60 GHz, 128 GB RAM).

5. Results and discussion

This section presents and discusses the main outcomes of this study. First, the kinematic analysis results, specifically the joint angle profiles, are compared among the prescribed data, the angle-based formulation, the Euler-based formulation, and, when available, literature data [50]. The influence of the selection of the relative Euler parameters to prescribe on the performance of the Euler-based formulation is also addressed. Next, the comparison of joint torques estimated from inverse dynamic analyses is presented. The computational efficiency of both formulations is then evaluated for kinematic and dynamic analyses across the different movements studied. Finally, the limitations of this study are discussed to provide a critical assessment of the results and to highlight potential directions for future work.

5.1. Kinematic analysis

For both formulations of the rotational driving constraints applied in this study, kinematic consistency was obtained across all movements, and no discontinuities were observed in the computed velocities and accelerations. The upper limb movements presented a high level of inter-subject variability, e.g. in performing pronation or supination of the RU joint during abduction in the frontal plane. Consequently, averaging data would not produce meaningful insights. As the findings were qualitatively similar across all eight test subjects, upper limb results are presented only for a single subject (male; 86 kg; 1.84 m) for simplicity.

No differences were observed in the SC, AC, and ST joint angles between the prescribed data, angle-based formulation, and Euler-based formulation, regardless of the movement evaluated. To illustrate the results for the GH, HU, and RU joints, their main joint angles are presented in Fig. 3 for the abduction in the frontal plane and the task of combing the hair. These two movements were selected to represent movement in different planes (frontal and sagittal) and to include a daily living task.

For both movements, the angle-based and Euler-based formulations closely reproduced the prescribed data for the GH elevation-depression, HU flexion-extension, and RU pronation-supination, with differences of $<3^\circ$ (Table 2). These small differences likely arise from simplifications in the multibody model. As the anatomical joints were modelled as ideal kinematic joints, secondary physiological rotations were not accounted for. Moreover, the joint rotation axes were not subject-specific, i.e., they did not account for the anatomical variations of the evaluated subjects [4]. This misalignment between the anatomical and model-defined axes of rotation at the HU and RU joints likely contributed to the larger discrepancies observed in these joints.

Figure 4 presents the flexion-extension of the right hip and knee joints and the dorsiflexion-plantarflexion of the right ankle (all primarily occurring in the sagittal plane). Similar to the upper limb, the Euler-based formulation produced results comparable to the angle-based formulation and the prescribed data, with the largest differences of 2.64° and 1.69° , respectively, observed in the knee joint near the peak amplitude of movement.

Table 2

Mean and maximum joint angle differences between the prescribed data and the rotational formulations tested for the movement of abduction in the frontal plane and combing the hair. The joint angles presented correspond to Glenohumeral (GH) elevation-depression, Humeroulnar (HU) flexion-extension, and Radioulnar (RU) pronation-supination.

Movement	Formulation	GH joint		HU joint		RU joint	
		Avg (°)	Max(°)	Avg (°)	Max(°)	Avg (°)	Max(°)
Abduction	Angle-based	0.00	0.00	1.07	2.08	0.31	0.68
	Euler-based	0.00	0.00	0.52	0.85	1.53	2.42
Combing the hair	Angle-based	0.00	0.00	0.80	1.70	0.29	0.57
	Euler-based	0.00	0.00	0.32	0.82	1.35	2.04

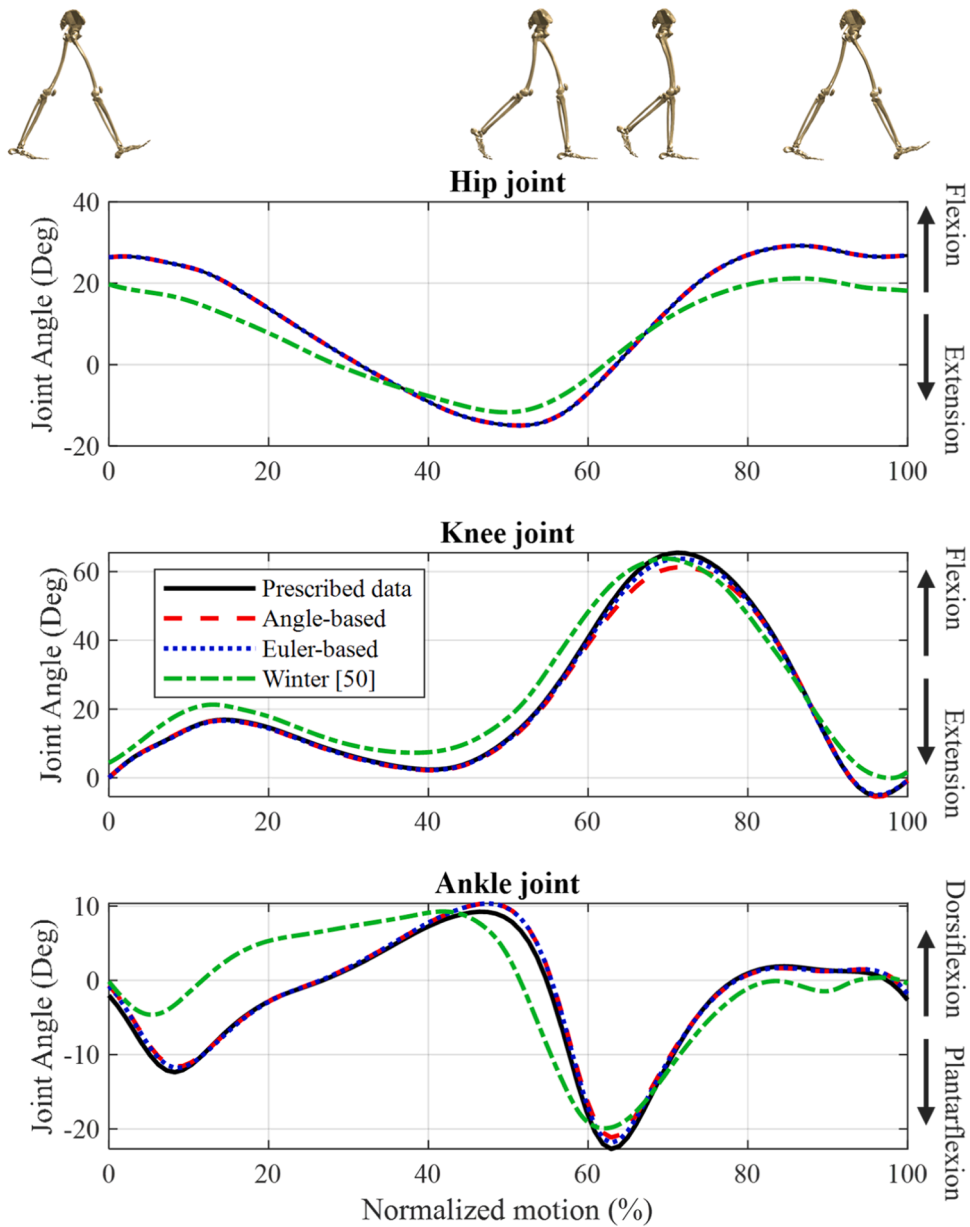


Fig. 4. Flexion-Extension of the hip and knee joints, and Dorsiflexion-Plantarflexion of the ankle joint, during a right gait cycle for the: prescribed data, angle-based formulation, Euler-based formulation, and literature data from Winter [50] for a normal cadence ($n = 19$).

The studied gait cycle exhibited the characteristically temporal and spatial patterns commonly documented in gait biomechanics literature [50]. However, minor differences were observed, likely influenced by the experimental set up. During data collection at the LBL, the subject was instructed to walk at a natural cadence while stepping on three force plates to acquire ground reaction forces. The need to step on the force plates may have influenced cadence, as reflected by a greater hip flexion (of about 5°) at heel strike and a greater hip hyperextension (about 8°) at terminal swing. The knee flexion-extension pattern followed the characteristic behaviour reported in the literature, with very low inter-subject variability [50]. For the ankle, the stance phase began with greater dorsiflexion, but the remainder of the gait cycle aligned well with literature data. Some of the observed differences may also stem from methodological disparities: this study used a 3D optoelectronic marker-based motion capture system to capture high-fidelity and multidimensional data on lower limb kinematics, while Winter [50] primarily evaluated gait kinematics in the sagittal (2D) plane using earlier measurement techniques.

5.1.1.1. Influence of relative Euler parameter selection on kinematics

The selection of relative Euler parameters to prescribe is not unique. While the components listed in Table 1 and certain alternatives

provided consistent and physiological results, some other selections led to two possible outcomes: (1) kinematic inconsistencies, in which the analysis failed to converge to positions that satisfied the kinematic constraints; or (2) kinematic consistency deviating from the prescribed motion, sometimes accompanied by unphysiological joint behaviour.

Figure 5 illustrates a case of knee joint deviation from the prescribed motion with unphysiological behaviour. When e_{1ij} was guided instead of e_{3ij} , the joint deviated from the measured data, leading to an amplitude of about 180° , which exceeds the physiological RoM of the knee, approximately 125° [51,52]. The knee also presented an hyperextension greater than 20° , which is not physiologically possible (in a healthy condition) [51,52]. Because the ξ -component of the knee's relative axis of rotation is small, as motion occurs primarily about the ζ -component, minor numerical inconsistencies (e.g., from data acquisition or model-subject differences) can cause deviations that must be compensated by the relative angle of rotation, thereby forcing the joint angle away from its expected path to satisfy the prescribed relative Euler parameter.

Another example of an improper choice of the relative Euler parameters is shown in Fig. 6 for the flexion-extension of the right hip joint, where the components e_{0ij} , e_{1ij} and e_{2ij} were prescribed. This combination constrains the relative angle of rotation (e_{0ij}) and two components of the relative axis of rotation (e_{1ij} and e_{2ij}). Because the third axis component is not explicitly prescribed, its sign remains ambiguous. This ambiguity cannot be resolved by e_{0ij} , since it encodes the rotation angle through a cosine term that is insensitive to sign. As a result, the motion exhibits a symmetric angle evolution when the joint angle passes through zero. In contrast, by guiding e_{1ij} , e_{2ij} and e_{3ij} , all three components of the relative axis of rotation are directly specified. Since the relative Euler parameters are normalized, this also implicitly defines the relative angle of rotation. Therefore, for three DoFs joints in open kinematic chains, the three components that explicitly define the orientation of the relative axis of rotation must be prescribed to fully and unambiguously control motion.

In closed kinematic chains, where the configuration of the bodies is interdependent, different combinations of the relative Euler parameters may, in theory, lead to the same overall kinematics within the chain. For example, the same motion could be achieved by prescribing one relative Euler parameter at the SC joint and three at the AC joint, or two at both the SC and AC joints. Additional simulations confirmed that some of these combinations produced consistent positions and followed the prescribed motion. However,

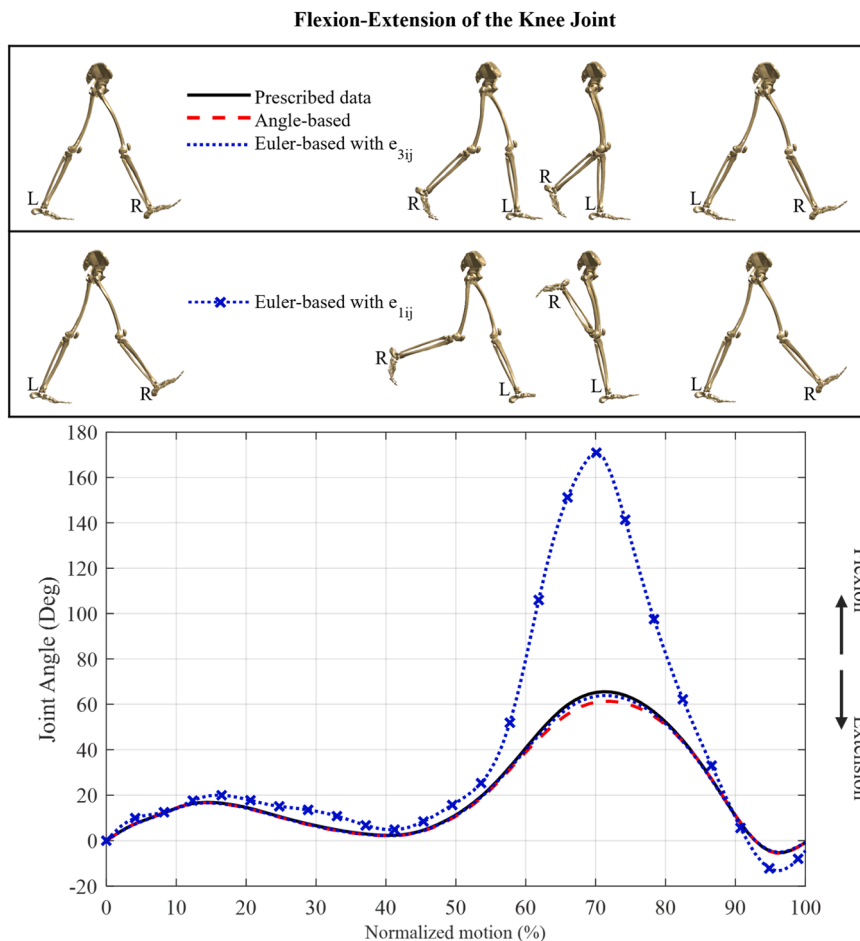


Fig. 5. Flexion-extension of the knee (in degrees) for the: prescribed data; angle-based formulation; and Euler-based formulation while guiding the component e_{3ij} , or e_{1ij} of the relative Euler parameters.

Flexion-Extension of the Hip Joint

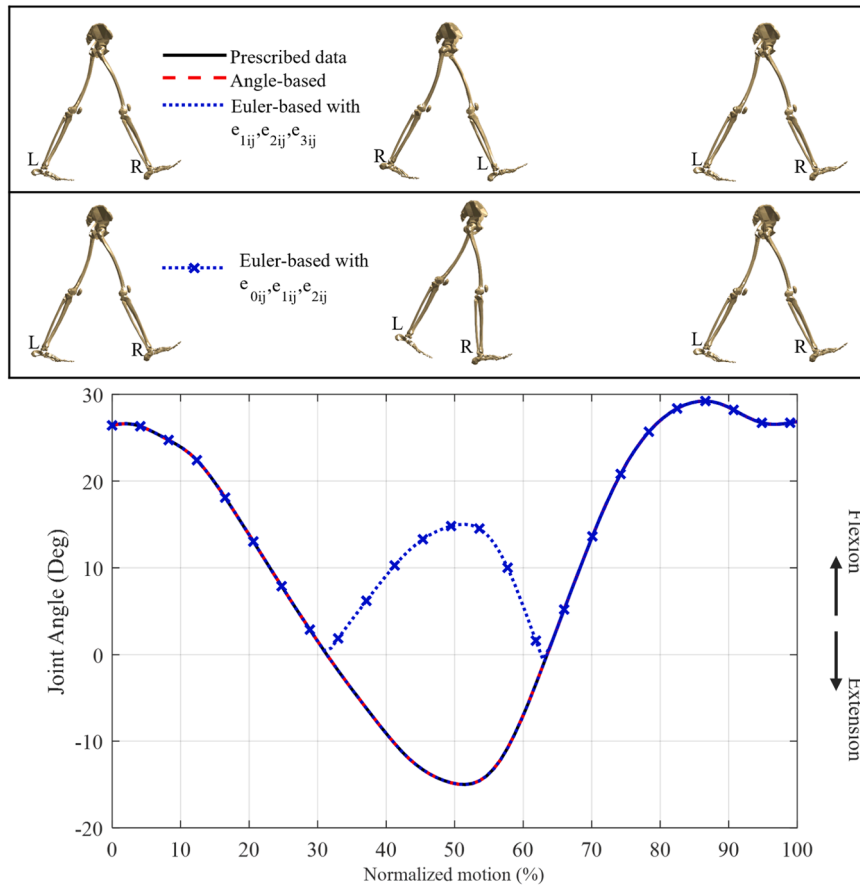


Fig. 6. Flexion-extension of the hip (in degrees) for the: prescribed data; angle-based formulation; and Euler-based formulation while guiding the components $e_{1ij}, e_{2ij}, e_{3ij}$, or the components $e_{0ij}, e_{1ij}, e_{2ij}$ of the relative Euler parameters.

most failed for movements outside of the frontal plane, such as forward flexion in the sagittal plane, reaching behind the back, or combing the hair. These findings indicate that closed kinematic chains may require chain-specific parameter selections or, alternatively, the development of dedicated formulations to ensure robust performance across a wider range of applications.

In summary, the choice of the relative Euler parameters to prescribe is inherently joint- and chain-dependent, meaning that full automation may not always be achievable and, in many cases, the selection still needs to be guided by the joint structure to ensure consistent and physiological kinematics.

5.2. Inverse dynamic analysis

The joint torques of the upper limb showed no meaningful differences between the angle-based and Euler-based formulations. As no literature data are available for comparison, these results are omitted for brevity.

Figure 7 presents the joint torques of the right hip, knee, and ankle obtained from inverse dynamic analysis, together with literature data. To enable comparison, the joint torques were normalized by body mass (75 kg). No relevant differences were observed between the Euler-based and angle-based formulations, and the estimated joint torques were consistent with those of the literature in both pattern and range. The hip joint presented the largest differences, which may be explained by its greater difference in joint angle range relative to the literature, as well as its higher inter-subject variability compared to the knee and ankle [50]. Additional discrepancies with literature data may also arise from differences in how the ground reaction forces and centres of pressure were measured and processed. In the present study, both were recorded synchronously with 3D motion capture using force plates, ensuring high-fidelity dynamic data. Variations in filtering procedures, sensor resolution, force plate characteristics, and algorithms for estimating the centres of pressure can all affect gait parameters. These methodological differences may contribute to the observed deviations from Winter's data, which were likely based on different force measurement and signal processing techniques [50]. Finally, it should be noted that the literature data represents an average of 19 joint torque patterns, whereas the computational data refers to a single test subject, which explains the smoother torque profiles observed in the literature.

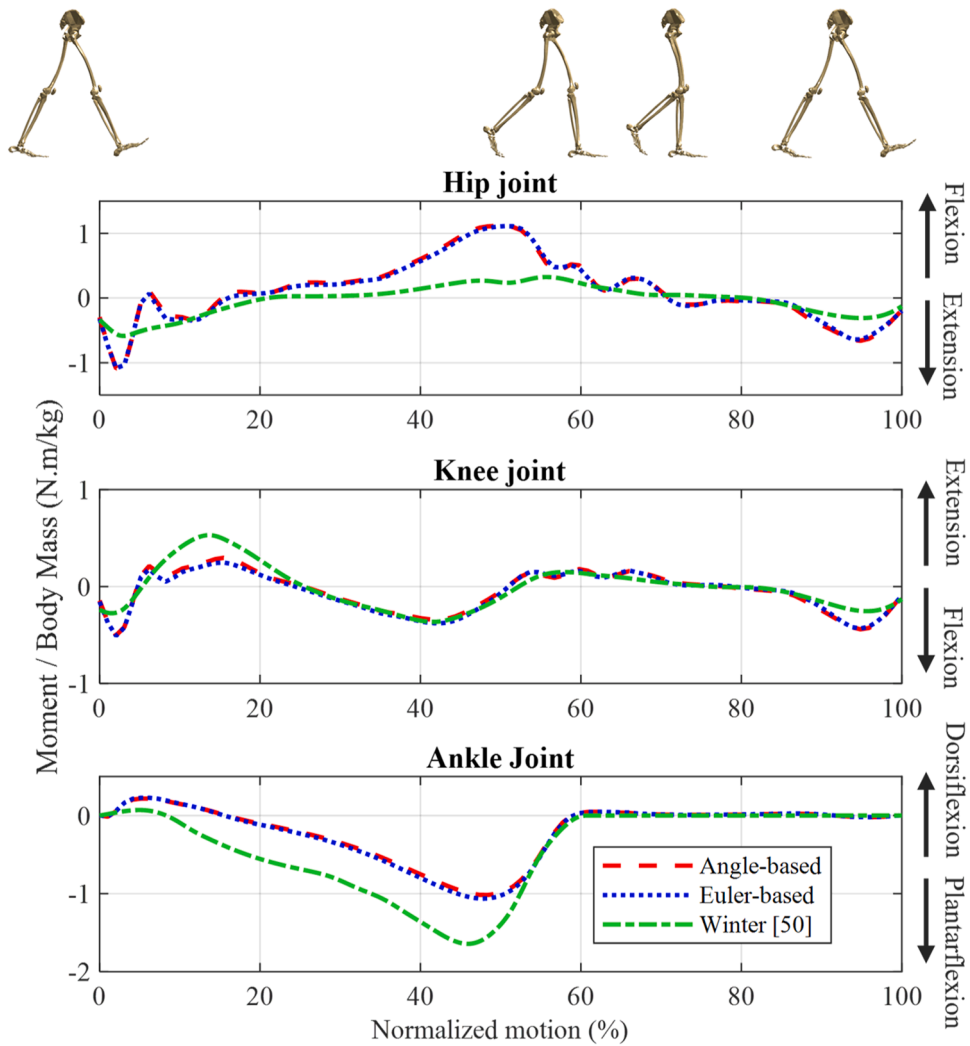


Fig. 7. Joint torques, normalized by body mass, for the hip and knee joints, during a right gait cycle for the: angle-based formulation, Euler-based formulation, and literature data from Winter [50] for a normal cadence ($n = 19$). Joint torques are reported as internal moments (proximal segment acting on distal segment) [53].

5.3. Computational efficiency

The truncated means of the computation times, computed after excluding the highest and lowest computation times, for the kinematic and dynamic analyses are shown in Table 3. Overall, the Euler-based formulation was faster than the angle-based formulation

Table 3

Truncated mean and standard deviation of the computational times (Mean \pm Std) for the angle-based and Euler-based formulations during kinematic and dynamic analyses. All computational times were normalized by the number of frames of the movement (ms/frame): abduction in the frontal plane (324 frames), flexion in the sagittal plane (352 frames), reaching behind the back (213 frames), combing the hair (286 frames), and a right gait cycle (118 frames).

Movement evaluated	Computational Time / Number of frames (ms/frame)					
	Kinematic constraints		Kinematic Analysis		Dynamic Analysis	
	Angle-based	Euler-based	Angle-based	Euler-based	Angle-based	Euler-based
Abduction	64	49	10.772 \pm 0.062	8.694 \pm 0.033	0.190 \pm 0.002	0.046 \pm 0.001
Flexion	64	49	11.848 \pm 0.053	8.747 \pm 0.028	0.179 \pm 0.001	0.045 \pm 0.001
Reaching behind the back	64	49	19.046 \pm 0.095	8.882 \pm 0.092	0.203 \pm 0.003	0.031 \pm 0.002
Combing the hair	64	49	11.974 \pm 0.039	8.818 \pm 0.087	0.202 \pm 0.004	0.036 \pm 0.008
Gait cycle	105	91	28.947 \pm 0.186	17.719 \pm 0.145	0.695 \pm 0.014	0.173 \pm 0.004

in both analyses. For the right upper limb, an average improvement of 31 % and 78 % was observed for the kinematic and inverse dynamic analyses, respectively. The improved performance is likely attributed to the lower number of kinematic constraint equations. The lower limb analyses required nearly twice the computation time of the upper limb analyses, reflecting their greater complexity: the angle-based and Euler-based formulations involved 105 and 91 kinematic constraints, respectively, in the lower limb analyses, compared to only 64 and 49 in the upper limb analyses.

5.4. Limitations

The continuous development of multibody model formulations is crucial, as these provide the means to estimate variables that are challenging or even impossible to measure directly in vivo or in vitro [4,54,55]. The Euler-based rotational driving constraint proposed in this study produced results consistent with both the angle-based formulation and literature data, for both kinematic and dynamic analyses. Unlike the angle-based formulation, which requires redundant constraints to handle singularities when the prescribed angle approaches zero, the Euler-based formulation operates without RoM limitations, offering a more robust framework.

Despite its advantages, the Euler-based formulation is not free of limitations. The selection of the relative Euler parameters to prescribe is not generic, as it depends on the specific characteristics of each joint, and closed kinematic chains require additional care. In this study, four upper limb movements were analysed across eight subjects, whereas only one gait cycle from a single subject was evaluated for the lower limbs. Given that the gait cycle is known to exhibit low inter-subject variability [50], and the Euler-based formulation showed good agreement with the literature data, both in terms of range and pattern, analysing a single subject for the lower limbs was deemed sufficient for the present evaluation. The performance of the Euler-based formulation was evaluated in kinematic and inverse dynamic analyses, but its performance in forward dynamics remains to be assessed. Nonetheless, based on its properties, no major issues are anticipated in the application of the Euler-based formulation to forward dynamic analyses.

6. Conclusion

This work discussed the formulation and implications of using Euler parameters for rotational driving constraints in multibody system dynamics. In the proposed Euler-based formulation, the Euler parameters describe the orientation of a body relative to another body, providing a consistent and singular representation of their relative motion. This approach produced independent kinematic constraints, avoiding the redundancy often observed when angles are used to prescribe relative rotation. To assess its performance, a three-dimensional (3D) multibody model of the human body was used together with kinematic data from upper and lower limb motions. The resulting joint kinematics and dynamics showed good agreement with both a traditional angle-based formulation and literature data, supporting the validity of the method. Moreover, the Euler-based formulation improved computational efficiency. Although the proposed formulation was tested in a biomechanical context, the underlying mathematical framework is general and can be applied to a wide range of multibody systems. Overall, the findings support the use of Euler parameters as an effective and reliable alternative to traditional angle-based formulations in multibody dynamics.

CRedit authorship contribution statement

Madalena Antunes: Writing – original draft, Visualization, Validation, Software, Methodology, Investigation, Formal analysis, Conceptualization. **João Folgado:** Writing – review & editing, Supervision, Project administration, Methodology, Investigation, Formal analysis, Conceptualization. **Carlos Quental:** Writing – review & editing, Supervision, Software, Resources, Project administration, Methodology, Investigation, Formal analysis, Conceptualization.

Declaration of competing interest

The authors declare that they have no known competing financial interests or personal relationships that could have appeared to influence the work reported in this paper.

Acknowledgments

The authors acknowledge Fundação para a Ciência e a Tecnologia (FCT) for its financial support via LAETA (project <https://doi.org/10.54499/UID/50022/2025>), and a PhD scholarship 2021.06844.BD.

Appendix A

Some identities with Euler parameters, time derivatives, and transformation matrices are important and useful in the derivation of the kinematic constraint equations. The matrices G and L are identities that relate to the Euler parameters by

$$\mathbf{G} = \begin{bmatrix} -e_1 & e_0 & -e_3 & e_2 \\ -e_2 & e_3 & e_0 & -e_1 \\ -e_3 & -e_2 & e_1 & e_0 \end{bmatrix} \quad (26)$$

$$\mathbf{L} = \begin{bmatrix} -e_1 & e_0 & e_3 & -e_2 \\ -e_2 & -e_3 & e_0 & e_1 \\ -e_3 & e_2 & -e_1 & e_0 \end{bmatrix} \quad (27)$$

These identities (\mathbf{G} and \mathbf{L}) also relate with the first time derivative of the Euler parameters:

$$\begin{aligned} \mathbf{G}\dot{\mathbf{p}} &= -\dot{\mathbf{G}}\mathbf{p} \quad , \quad \mathbf{L}\dot{\mathbf{p}} = -\dot{\mathbf{L}}\mathbf{p} \\ \dot{\mathbf{G}}\dot{\mathbf{p}} &= \dot{\mathbf{L}}\dot{\mathbf{p}} = \mathbf{0} \\ \mathbf{G}\dot{\mathbf{L}}^T &= \dot{\mathbf{G}}\mathbf{L}^T \end{aligned} \quad (28)$$

Considering an arbitrary 3-entry vector, the matrices $\overset{+}{\mathbf{a}}$ and $\bar{\mathbf{a}}$ are skew-matrices and can be written as

$$\overset{+}{\mathbf{a}} = \begin{bmatrix} 0 & -\mathbf{a}^T \\ \mathbf{a} & \tilde{\mathbf{a}} \end{bmatrix} \quad \bar{\mathbf{a}} = \begin{bmatrix} 0 & -\mathbf{a}^T \\ \mathbf{a} & -\tilde{\mathbf{a}} \end{bmatrix} \quad (29)$$

These matrices and arbitrary vectors are used to relate the matrices \mathbf{G} and \mathbf{L} with the Euler parameters and respective time derivatives:

$$\begin{aligned} \mathbf{G}^T \mathbf{a} &= \overset{+}{\mathbf{a}}\mathbf{p} \quad , \quad \mathbf{L}^T \mathbf{a} = \bar{\mathbf{a}}\mathbf{p} \\ \dot{\mathbf{G}}^T \mathbf{a} &= \overset{+}{\dot{\mathbf{a}}}\mathbf{p} \quad , \quad \dot{\mathbf{L}}^T \mathbf{a} = \bar{\dot{\mathbf{a}}}\mathbf{p} \\ \ddot{\mathbf{G}}^T \mathbf{a} &= \overset{+}{\ddot{\mathbf{a}}}\mathbf{p} \quad , \quad \ddot{\mathbf{L}}^T \mathbf{a} = \bar{\ddot{\mathbf{a}}}\mathbf{p} \end{aligned} \quad (30)$$

If the generalized velocities and accelerations are expressed in terms of angular velocities or accelerations, respectively, they can also be related with the Euler parameters, their time derivatives, and the identities \mathbf{G} and \mathbf{L} through:

$$\boldsymbol{\omega} = 2\mathbf{G}\dot{\mathbf{p}} \quad , \quad \dot{\mathbf{p}} = \frac{1}{2}\mathbf{G}^T\boldsymbol{\omega} \quad (31)$$

$$\boldsymbol{\omega}' = 2\mathbf{L}\dot{\mathbf{p}} \quad , \quad \dot{\mathbf{p}} = \frac{1}{2}\mathbf{L}^T\boldsymbol{\omega}'$$

$$\dot{\boldsymbol{\omega}} = 2\mathbf{G}\ddot{\mathbf{p}} \quad , \quad \ddot{\mathbf{p}} = \frac{1}{2}\mathbf{G}^T\dot{\boldsymbol{\omega}} - \frac{1}{4}(\boldsymbol{\omega}^T\boldsymbol{\omega})\mathbf{p} \quad (32)$$

$$\dot{\boldsymbol{\omega}}' = 2\mathbf{L}\ddot{\mathbf{p}} \quad , \quad \ddot{\mathbf{p}} = \frac{1}{2}\mathbf{L}^T\dot{\boldsymbol{\omega}}' - \frac{1}{4}(\boldsymbol{\omega}'^T\boldsymbol{\omega}')\mathbf{p}$$

Appendix B

When describing the orientation of a body i with respect to a body j using relative Euler parameters, the identities \mathbf{G} and \mathbf{L} of each body and their Euler parameters are related through:

$$\begin{aligned} \mathbf{L}_i\mathbf{p}_j &= -\mathbf{L}_j\mathbf{p}_i \\ \mathbf{G}_i\mathbf{p}_j &= -\mathbf{G}_j\mathbf{p}_i \end{aligned} \quad (33)$$

Similarly, the time derivatives of the identities \mathbf{G} and \mathbf{L} of each body are related to the time derivatives of their Euler parameters by:

$$\begin{aligned} \mathbf{L}_i\dot{\mathbf{p}}_j &= -\dot{\mathbf{L}}_j\mathbf{p}_i \\ \mathbf{G}_i\dot{\mathbf{p}}_j &= -\dot{\mathbf{G}}_j\mathbf{p}_i \end{aligned} \quad (34)$$

The first and second time derivatives of matrices \mathbf{G} and \mathbf{L} are equal to constructing them, using Eqs. (26) and (27), respectively, with the first or second time derivatives of the Euler parameters:

$$\begin{aligned} \dot{\mathbf{L}} &= \mathbf{L}(\dot{\mathbf{p}}) \quad , \quad \ddot{\mathbf{L}} = \mathbf{L}(\ddot{\mathbf{p}}) \\ \dot{\mathbf{G}} &= \mathbf{G}(\dot{\mathbf{p}}) \quad , \quad \ddot{\mathbf{G}} = \mathbf{G}(\ddot{\mathbf{p}}) \end{aligned} \quad (35)$$

The first time derivative of the Euler-based rotational driving constraint equation, expressed in Eq. (19), is given by:

$$\overset{\cdot}{\Phi}^{(E-\text{rot},1)} = \mathbf{0} \Leftrightarrow \mathbf{v}^T\dot{\mathbf{p}}_{ij} - \dot{\mathbf{e}}^*(t) = \mathbf{0} \Leftrightarrow \mathbf{v}^T\dot{\mathbf{p}}_{ij} = \dot{\mathbf{e}}^*(t) \quad (36)$$

where the right-hand side represents the right-hand side vector of the velocity constraint equations, as presented in Eq. (23). Considering the relationships presented in Eqs. (31) and (34), the first time derivative of the relative Euler parameters can be expressed as:

$$\begin{aligned}\dot{\mathbf{p}}_{ij} &= \begin{bmatrix} \dot{\mathbf{p}}^T \\ \dot{\mathbf{L}} \end{bmatrix}_j \mathbf{p}_i + \begin{bmatrix} \mathbf{p}^T \\ \mathbf{L} \end{bmatrix}_j \dot{\mathbf{p}}_i = \begin{bmatrix} \mathbf{p}^T \\ \mathbf{L} \end{bmatrix}_j \dot{\mathbf{p}}_i + \begin{bmatrix} \dot{\mathbf{p}}^T \mathbf{p}_i \\ \dot{\mathbf{L}}_j \mathbf{p}_i \end{bmatrix} \\ &= \begin{bmatrix} \mathbf{p}^T \\ \mathbf{L} \end{bmatrix}_j \dot{\mathbf{p}}_i + \begin{bmatrix} \mathbf{p}^T \\ -\mathbf{L} \end{bmatrix}_i \dot{\mathbf{p}}_j\end{aligned}\quad (37)$$

Substituting this expression into Eq. (36) yields, on the left-hand side, the Jacobian matrix of the rotational driving constraint, as presented in Eq. (21). Using the relationships given in Eq. (31), the first time derivative of the relative Euler parameters can also be expressed in terms of the angular velocities $\boldsymbol{\omega}'$:

$$\dot{\mathbf{p}}_{ij} = \frac{1}{2} \begin{bmatrix} \mathbf{p}^T \\ \mathbf{L} \end{bmatrix}_j \mathbf{L}_i^T \boldsymbol{\omega}'_i + \frac{1}{2} \begin{bmatrix} \mathbf{p}^T \\ -\mathbf{L} \end{bmatrix}_i \mathbf{L}_j^T \boldsymbol{\omega}'_j\quad (38)$$

The second time derivative of the Euler-based constraint equation, or the first time derivative of the velocity constraint equation, can be written as:

$$\begin{aligned}\ddot{\Phi} &= 0 \\ \mathbf{v}^T \begin{bmatrix} \dot{\mathbf{p}}^T \\ \dot{\mathbf{L}} \end{bmatrix}_j \dot{\mathbf{p}}_i + \mathbf{v}^T \begin{bmatrix} \mathbf{p}^T \\ \mathbf{L} \end{bmatrix}_j \ddot{\mathbf{p}}_i + \mathbf{v}^T \begin{bmatrix} \dot{\mathbf{p}}^T \\ -\dot{\mathbf{L}} \end{bmatrix}_i \dot{\mathbf{p}}_j + \mathbf{v}^T \begin{bmatrix} \mathbf{p}^T \\ -\mathbf{L} \end{bmatrix}_i \ddot{\mathbf{p}}_j - \ddot{\mathbf{e}}^*(t) &= 0\end{aligned}\quad (39)$$

As in the velocity constraint equations, moving all terms that do not involve accelerations to the right-hand side yields the right-hand side vector of the acceleration equations, as expressed in Eq. (24). Using the relationships presented in Eq. (32), and applying the same procedure to isolate the terms independent of accelerations, the right-hand side vector of the acceleration constraint equations written in terms of angular accelerations $\dot{\boldsymbol{\omega}}'$ is obtained, as expressed in Eq. (25).

Data availability

Data will be made available on request.

References

- [1] W. Schiehlen, Research trends in multibody system dynamics, *Multibody Syst. Dyn.* 18 (2007) 3–13, <https://doi.org/10.1007/s11044-007-9064-4>.
- [2] J. García de Jalón, E. Bayo, *Kinematic and Dynamic Simulation of Multibody Systems: the Real-Time Challenge*, Springer, New York, 1994.
- [3] P.E. Nikravesh, *Computer-aided Analysis of Mechanical Systems*, Prentice-Hall, Englewood Cliffs, N.J., 1988.
- [4] I. Roupa, M.R. da Silva, F. Marques, S.B. Gonçalves, P. Flores, M.T. da Silva, On the modeling of biomechanical systems for Human movement analysis: a narrative review, *Arch. Comput. Methods Eng.* 29 (2022) 4915–4958, <https://doi.org/10.1007/s11831-022-09757-0>.
- [5] S.B. Gonçalves, I. Roupa, P. Flores, M.T. da Silva, Kinematic and inverse dynamic analysis using mixed and fully cartesian coordinates with a generic rigid body, *Mech. Mach. Theory* 214 (2025) 106080, <https://doi.org/10.1016/j.mechmachtheory.2025.106080>.
- [6] E.J. Haug, *Computer Aided Kinematics and Dynamic of Mechanical Systems*, Allyn and Bacon, 1989.
- [7] J.M. Hansen, Planar multibody systems, in: J.A.C. Ambrósio, P. Eberhard (Eds.), *Advanced Design of Mechanical Systems: From Analysis to Optimization*, Springer Vienna, Vienna, 2009; pp. 1–21. <https://doi.org/10.1007/978-3-211-99461-0>.
- [8] P.E. Nikravesh, R.A. Wehage, O.K. Kwon, Euler parameters in computational kinematics and dynamics. Part 1, *J. Mech. Transm. Autom. Des.* 107 (1985) 358–365, <https://doi.org/10.1115/1.3260722>.
- [9] A.A. Shabana, *Dynamics of Multibody Systems*, 4th Edition, Cambridge University Press, 2013.
- [10] F. Reuleaux, *Kinematics of Machinery*, MacMillan and Co., 1963.
- [11] R. Dumas, L. Chèze, 3D inverse dynamics in non-orthonormal segment coordinate system, *Med. Biol. Eng. Comput.* 45 (2007) 315–322, <https://doi.org/10.1007/s11517-006-0156-8>.
- [12] M.P.T. Silva, J.A.C. Ambrósio, Kinematic data consistency in the inverse dynamic analysis of biomechanical systems, *Multibody Syst. Dyn.* 8 (2002) 219–239, <https://doi.org/10.1023/A:1019545530737>.
- [13] A. Czaplicki, M.T. Silva, J.C. Ambrósio, Biomechanical modelling for whole body motion using natural coordinates, *J. Theor. Appl. Mech.* 42 (2004) 927–944.
- [14] S.E. Rodrigo, J.A.C. Ambrósio, A biomechanical approach to characterize neural coordination during gait, in: *Multibody Dynamics 2011, ECCOMAS Thematic Conference*, 2011. <https://www.researchgate.net/publication/260164907>.
- [15] R. Huston, C. Passerello, Multibody dynamics including translation between the bodies - with application to head-neck systems, 1978.
- [16] J. García de Jalón, E. Bayo, *Kinematic and Dynamic Simulation of Multibody Systems*, Springer New York, New York, NY, 1994, <https://doi.org/10.1007/978-1-4612-2600-0>.
- [17] I. Roupa, S.B. Gonçalves, M.T. da Silva, Kinematics and dynamics of planar multibody systems with fully Cartesian coordinates and a generic rigid body, *Mech. Mach. Theory* 180 (2023) 105134, <https://doi.org/10.1016/j.mechmachtheory.2022.105134>.
- [18] J. García de Jalón, M.D. Gutiérrez-López, Multibody dynamics with redundant constraints and singular mass matrix: existence, uniqueness, and determination of solutions for accelerations and constraint forces, *Multibody Syst. Dyn.* 30 (2013) 311–341, <https://doi.org/10.1007/s11044-013-9358-7>.
- [19] P.E. Nikravesh, E.J. Haug, Generalized coordinate partitioning for analysis of mechanical systems with nonholonomic constraints, *J. Mech. Transm. Autom. Des.* 105 (1983) 379–384. <http://www.asme.org/about-asme/terms-of-use>.
- [20] E. Bayo, R. Ledesma, Augmented lagrangian and mass-orthogonal projection methods for constrained multibody dynamics, *Nonlin. Dyn.* 9 (1996) 113–130.
- [21] E. Bayo, A. Avello, Singularity-free augmented lagrangian algorithms for constrained multibody dynamics, *Nonlin. Dyn.* 5 (1994) 209–231.
- [22] N. Potosakis, E. Paraskevopoulos, S. Natsiavas, Application of an augmented Lagrangian approach to multibody systems with equality motion constraints, *Nonlin. Dyn.* 99 (2020) 753–776, <https://doi.org/10.1007/s11071-019-05059-6>.
- [23] B. Ruzzeh, J. Kóvecses, A penalty formulation for dynamics analysis of redundant mechanical systems, *J. Comput. Nonl. Dyn.* 6 (2011), <https://doi.org/10.1115/1.4002510>.

- [24] L. Yang, S. Xue, W. Yao, Application of Gauss principle of least constraint in multibody systems with redundant constraints, *Proc. Inst. Mech. Eng. K: J Multi-Body Dyn.* 235 (2021) 150–163, <https://doi.org/10.1177/1464419320975301>.
- [25] L. Euler, *Formulae generales pro translatione quacunque corporum rigidorum*, *Novi. Comment. Acad. Sci. Petropolitanae* 20 (1776) 189–207, 20.
- [26] J. Pujol, Hamilton, Rodrigues, Gauss, Quaternions, and rotations: a historical reassessment, *Commun. Math. Anal.* 13 (2012) 1–14.
- [27] R. Friedberg, Rodrigues, Olinda: des lois geometriques qui regissent les déplacements dun systeme solide, *Transl. Comment.* (2022).
- [28] J. Wittenburg, *Dynamics of Multibody Systems*, Springer, 2008.
- [29] P.E. Nikravesh, I.S. Chung, Application of euler parameters to the dynamic analysis of three-dimensional constrained mechanical systems, *J. Mech. Des.* 104 (1982) 785–791, <https://doi.org/10.1115/1.3256437>.
- [30] P.E. Nikravesh, O.K. Kwon, R.A. Wehage, Euler parameters in computational kinematics and dynamics. Part 2, *J. Mech. Transm. Autom. Des.* 107 (1985) 366–369, <https://doi.org/10.1115/1.3260723>.
- [31] M.F.O. Seabra Pereira, J.A.C. Ambrósio, *Computer-Aided Analysis of Rigid and Flexible Mechanical Systems*, Springer Netherlands, Dordrecht, 1994, <https://doi.org/10.1007/978-94-011-1166-9>.
- [32] K.M. Noh, D.C. Erbauch, A semi-recursive dynamic algorithm using variational vector approach, *Trans. ASAE* 34 (1991) 1566–1574, <https://doi.org/10.13031/2013.31771>.
- [33] D.-L. Tsai, *A General Purpose Rigid Body Dynamic Analysis Program With Applications to Control of Zero Angular Momentum Turns*, University of Arizona, 1990.
- [34] C. Quental, J. Folgado, J. Ambrósio, J. Monteiro, A multibody biomechanical model of the upper limb including the shoulder girdle, *Multibody Syst. Dyn.* 28 (2012) 83–108, <https://doi.org/10.1007/s11044-011-9297-0>.
- [35] C. Quental, J. Folgado, J. Ambrósio, A window moving inverse dynamics optimization for biomechanics of motion, *Multibody Syst. Dyn.* 38 (2016) 157–171, <https://doi.org/10.1007/s11044-016-9529-4>.
- [36] W. Schiehlen, *Multibody system dynamics: roots and perspectives*, *Multibody Syst. Dyn.* 1 (1997) 149–188, <https://doi.org/10.1023/A:1009745432698>.
- [37] R. Featherstone, *Rigid Body Dynamics Algorithms*, Springer US, Boston, MA, 2008, <https://doi.org/10.1007/978-1-4899-7560-7>.
- [38] P. Flores, *Concepts and Formulations for Spatial Multibody Dynamics*, Springer International Publishing, Cham, 2015, <https://doi.org/10.1007/978-3-319-16190-7>.
- [39] F.C.T. van der Helm, *The Shoulder mechanism: a Dynamic Approach*, Delft University of Technology, 1991. Doctoral thesis.
- [40] A. Rajagopal, C.L. Dembia, M.S. DeMers, D.D. Delp, J.L. Hicks, S.L. Delp, Full-body musculoskeletal model for muscle-driven simulation of Human gait, *IEEE Trans. Biomed. Eng.* 63 (2016) 2068–2079, <https://doi.org/10.1109/TBME.2016.2586891>.
- [41] G. Wu, S. Siegler, P. Allard, C. Kirtley, A. Leardini, D. Rosenbaum, M. Whittle, D.D. D’Lima, L. Cristofolini, H. Witte, O. Schmid, I. Stokes, ISB recommendation on definitions of joint coordinate system of various joints for the reporting of human joint motion - part I: ankle, hip and spine, *J. Biomech.* 35 (2002) 543–548, [https://doi.org/10.1016/S0021-9290\(01\)00222-6](https://doi.org/10.1016/S0021-9290(01)00222-6).
- [42] G. Wu, F.C.T. Van Der Helm, H.E.J. Veeger, M. Makhssous, P. Van Roy, C. Anglin, J. Nagels, A.R. Karduna, K. McQuade, X. Wang, F.W. Werner, B. Buchholz, ISB recommendation on definitions of joint coordinate systems of various joints for the reporting of human joint motion - part II: shoulder, elbow, wrist and hand, *J. Biomech.* 38 (2005) 981–992, <https://doi.org/10.1016/j.jbiomech.2004.05.042>.
- [43] D. Winter, *Biomechanics and Motor Control of Human Movement*, 4th ed., Wiley, Ontario, Canada, 2009.
- [44] S.S.H.U. Gamage, J. Lasenby, New least squares solutions for estimating the average centre of rotation and the axis of rotation, *J. Biomech.* 35 (2002) 87–93, [https://doi.org/10.1016/S0021-9290\(01\)00160-9](https://doi.org/10.1016/S0021-9290(01)00160-9).
- [45] R. Hara, J. McGinley, C. Briggs, R. Baker, M. Sangeux, Predicting the location of the hip joint centres, impact of age group and sex, *Sci. Rep.* 6 (2016) 37707, <https://doi.org/10.1038/srep37707>.
- [46] A.F. Shaheen, C.M. Alexander, A.M.J. Bull, Effects of attachment position and shoulder orientation during calibration on the accuracy of the acromion tracker, *J. Biomech.* 44 (2011) 1410–1413, <https://doi.org/10.1016/j.jbiomech.2011.01.013>.
- [47] A. Cereatti, C. Rosso, A. Nazarian, J.P. DeAngelis, A.J. Ramappa, U. Della Croce, Scapular motion tracking using acromion skin marker cluster: in vitro accuracy assessment, *J. Med. Biol. Eng.* 35 (2015) 94–103, <https://doi.org/10.1007/s40846-015-0010-2>.
- [48] F.C.T. van der Helm, G.M. Pronk, Three-dimensional recording and description of motions of the shoulder mechanism, *J. Biomech. Eng.* 117 (1995) 27–40, <https://doi.org/10.1115/1.2792267>.
- [49] J.A.I. Prinold, A.M.J. Bull, Scaling and kinematics optimisation of the scapula and thorax in upper limb musculoskeletal models, *J. Biomech.* 47 (2014) 2813–2819, <https://doi.org/10.1016/j.jbiomech.2014.05.015>.
- [50] D.A. Winter, *The Biomechanics and Motor Control of Human Gait*, University of Waterloo Press, 1987.
- [51] A. Bolukbasi, D.E. Laananen, Application of the nonlinear finite element method to crashworthiness analysis of aircraft seats, in: 24th Structures, Structural Dynamics and Materials Conference, American Institute of Aeronautics and Astronautics, Reston, Virginia, 1983, <https://doi.org/10.2514/6.1983-929>.
- [52] J. Panero, M. Zelnik, *Human Dimension and Interior Space*, Watson-Guptill, 1979.
- [53] T.R. Derrick, A.J. van den Bogert, A. Cereatti, R. Dumas, S. Fantozzi, A. Leardini, ISB recommendations on the reporting of intersegmental forces and moments during human motion analysis, *J. Biomech.* 99 (2020) 109533, <https://doi.org/10.1016/j.jbiomech.2019.109533>.
- [54] C. Quental, J. Folgado, J. Ambrósio, J. Monteiro, Multibody system of the upper limb including a reverse shoulder prosthesis, *J. Biomech. Eng.* 135 (2013), <https://doi.org/10.1115/1.4025325>.
- [55] M. Antunes, C. Quental, J. Folgado, A.C. Ângelo, C. de Campos Azevedo, Influence of the rotator cuff tear pattern in shoulder stability after arthroscopic superior capsule reconstruction: a computational analysis, *J. ISAKOS* 9 (2024) 296–301, <https://doi.org/10.1016/j.jisako.2024.01.014>.